WIS-95/11/Mar-PH

Description of inclusive scattering of few-GeV electrons from finite A nuclei and nuclear matter

A.S. Rinat and M.F. Taragin

Department of Particle Physics, Weizmann Institute of Science, Rehovot 76100, Israel

(April 11, 1995)

Abstract

We study eA scattering in a model where the total nuclear structure function is a convolution of components W_N for an isolated nucleon and $W_{\rm N/A}$ for a nucleus composed of point-nucleons. W_N is represented by its elastic and lowest-energy inelastic parts, while $W_{\rm N/A}$ is computed from its asymptotic limit, supplemented by final state interactions due to binary collisions between the knocked-out and core nucleons. $(q/M)W_{\rm N/A}$ per nucleon appears to be practically independent of mass number A and momentum transfer q. Consequently, predicted inclusive cross sections per nucleon for given kinematic conditions hardly depend on the target and the same can be extracted from the data. Exceptions are low energy loss regions, where relatively small cross sections are shown to be sensitive to details of the single nucleon momentum distribution and to FSI, involving multiple collisions. The agreement with the data is good.

Typeset using REVTEX

Over the past few years a substantial body of data has been taken on cross sections for inclusive scattering of electrons from various nuclei. We concentrate on the SLAC-Virginia data for the following incident electron energies and scattering angles [1–3]: ϵ= 2.0 GeV, $\theta = 15°, 20°$; ϵ= 3.6 GeV, $\theta = 16°, 20°, 25°, 30°$; ϵ= 4.0 GeV, $\theta = 30°$, each for a range of energy losses ν. Those sets span 3- and 4-momentum transfers $q^2 \lesssim 4.8$ GeV^2 and $Q^2 \lesssim 3.35$ GeV^2 respectively. Targets were He,C, Al, Fe and Au, while quasi-data for nuclear matter (NM) have been generated by extrapolation of the above to $A \to \infty$ [4]. Below we shall give a description, addressing in particular the physical content of this large body of data.

Until now virtually all approaches are based on the Plane Wave Impulse Approximation (PWIA), where for high q the interaction of the core with the knocked-out proton is neglected. Central in the PWIA is the single-hole spectral function. Except for NM [5], accurate results exist only for light nuclei (cf. [6]) and for general A one has to resort to approximations. The latter range from selected, parametrized one-hole and two-hole, single particle contributions [7], to a local density approximation based on NM results [8]. Beyond the PWIA one eventually adds Final State Interactions (FSI) leading to a Distorted Wave Impulse Approximation (DWIA). That result, corrected for estimated colour transparency effects, has been compared with the above data [8–10].

In an alternative approach for NM we start from the large-q limit of the underlying structure function or response [11]. Contrary to the IA, there exists for non-relativistic (NR) dynamics, a systematic way to incorporate FSI contributions beyond the asymptotic limit [12]. Since the final expressions for responses contain only observables with no explicit reference to the underlying NR dynamics, those have been assumed to be valid in general.

The above-mentioned approach for NM may be generalized for finite-A nuclei. Yet we prefer a somewhat different variant which we now expound. We start with the Rosenbluth cross section for inclusive scattering unpolarized electrons on a target of A composite nucleons

$$\frac{d^2\sigma_{eA}}{d\Omega d\epsilon'} = \left(\frac{d\sigma}{d\Omega}\right)_{\rm M}\Big[W_{2,A}(q,\nu) + 2{\rm tg}^2(\theta/2)W_{1,A}(q,\nu)\Big]$$

$$\left(\frac{d\sigma}{d\Omega}\right)_{\rm M} = 4\alpha^2\epsilon'^2\cos^2(\theta/2)/Q^4, \tag{1}$$

where ϵ', Ω are the measured electron final energy and scattering angular volume. W_A are total nuclear structure functions, which have to be computed for a nucleus consisting of, in principle, composite nucleons. Those functions we represent below by a convolution of two parts: $W_{\rm N/A}$ for a nucleus made up of point-nucleons and W_N for a composite nucleon, each relating to different degrees of freedom. With $\mathcal{E}_{\boldsymbol{q}}$ the nucleon recoil energy we thus write $(i = 1, 2)$

$$W_{i,A}(q,\nu) = \int d\nu' W_{\rm N/A}(q, \nu - \nu' + \mathcal{E}_{\boldsymbol{q}}) W_{i,N}(q,\nu') \tag{2}$$

Expressions of the form (2) have been proven in special cases, for instance in the PWIA [13]. It is also a non-perturbative exact result for a NR quark-cluster model and the structure functions there refer to on-shell targets at rest. An adapted form has been conjectured to hold generally [14].

Eq. (2) permits the use of actual data for W_N, but for the kinematic conditions of the SLAC experiment it suffices to select those components where the nucleon remains in its ground state or is at most excited to a Δ. Then with $\eta = Q^2/4M^2$ and $G_{E,M}$, the standard elastic form factors one has

$$W_N = W_N^{el} + W_N^{inel} \tag{3a}$$

$$W_N^{el} = \bar{W}_N^{el}\delta(\nu - Q^2/2M) \tag{3b}$$

$$\bar{W}_N^{el} = \left[\frac{G_E^2(Q^2) + \eta G_M^2(Q^2)}{1+\eta} + 2\eta G_M^2(Q^2){\rm tg}^2(\theta/2)\right] \tag{3c}$$

In contradistinction to W_N, $W_{\rm N/A}$ has to be computed. We do so with emphasis on FSI due to collisions between the high-momentum knocked-out nucleon and low-momentum core nucleons. For NR dynamics Gersch et al. derived for the reduced response per nucleon [12]

$$\phi(q,y) = (q/M)W_{\rm N/A} = \int \frac{d\boldsymbol{p}}{(2\pi)^3} n(p) R\Big(q, \frac{M}{q}\Big[\nu - \frac{Q^2}{2M} - \frac{\boldsymbol{p}.\boldsymbol{q}}{M}\Big]\Big) \tag{4a}$$

$$= \int \frac{d\boldsymbol{p}}{(2\pi)^3} n(p) R(q, y - p_z) \tag{4b}$$

The above describes the reduced response $\phi(q, y)$ of a a nucleon with momentum $\boldsymbol{p}$ which, after absorption of the 4-momentum q of the virtual photon, undergoes FSI contained in R. The expression is then folded into the distribution $n(p)$ of the initial momenta of the nucleon. Eq. (4b) makes explicit the replacement of the energy transfer ν by a (relativistic) scaling variable [15]

$$y = (y_W) \approx \frac{M}{q}\Big(\nu - \frac{Q^2}{2M} + \frac{\langle\Delta\rangle\nu}{M}\Big) \approx \frac{M}{q}\Big(\nu - \frac{Q^2}{2M}\Big), \tag{5}$$

$\langle\Delta\rangle$ is some average separation energy, which is negligible except in the immediate neighbourhood of the Quasi-Elastic Peak (QEP) $y \approx 0$, $\nu \approx Q^2/2M$.

FSI effects vanish in the asymptotic limit $q \to \infty$ and corresponds to $R(q, y - p_z) \to \delta(y - p_z)$ [12] and therefore

$$\phi^{as}(y) = 2\pi \int_{|y|}^{\infty} dppn(p) \tag{6}$$

Our major concern is the FSI factor R in (4) for finite q. For NR dynamics with interactions V between constituents there exists a systematic expansion in $1/q$ of the dominant incoherent part of $W_{\mathrm{N/A}}$ [12]. With $v_q = q/M$

$$\phi^{NR}(q, y) = \int \frac{ds}{2\pi} e^{iys} \tilde{\phi}^{NR}(q, s) \tag{7a}$$

$$\begin{aligned}\tilde{\phi}^{NR}(q, s) = \int d\boldsymbol{r}_1 \Big[\rho_1(\boldsymbol{r}_1, \boldsymbol{r}_1 - s\hat{\boldsymbol{q}}) + \frac{i}{v_q} \int d\boldsymbol{r}_2 \rho_2(\boldsymbol{r}_1, \boldsymbol{r}_2; \boldsymbol{r}_1 - s\hat{\boldsymbol{q}}, \boldsymbol{r}_2) \\ \Big(\int_0^s ds' V(\boldsymbol{r}_1 - \boldsymbol{r}_2 - s'\hat{q}) - sV(\boldsymbol{r}_1 - \boldsymbol{r}_2 - s\hat{q})\Big) + ...\Big]\end{aligned} \tag{7b}$$

$$= \int d\boldsymbol{r}_1 \rho_1(\boldsymbol{r}_1, \boldsymbol{r}_1 - s\hat{\boldsymbol{q}}) \exp[\tilde{\Omega}(q, \boldsymbol{r}_1, s)] \tag{7c}$$

The above expression contains density-matrices $\rho_n(\boldsymbol{r}_1, \boldsymbol{r}_1'; \boldsymbol{r}_j)$ of any order n which are diagonal in all coordinates $2 \leq j \leq n$, except in the coordinate 1 of the struck particle. For ρ_1 we use the Negele-Vautherin Ansatz [16].

$$\rho_1(\boldsymbol{r}_1, \boldsymbol{r}_1') \approx \rho(S)\Sigma(s) \approx \rho(\boldsymbol{r}_1) \int \frac{d\boldsymbol{p}}{(2\pi)^3} e^{-i\boldsymbol{p}.\boldsymbol{s}} n(p), \tag{8}$$

where $\boldsymbol{S} = (\boldsymbol{r}_1 + \boldsymbol{r}_1')/2$, $\boldsymbol{s} = \boldsymbol{r}_1 - \boldsymbol{r}_1'$; $\rho(r) = \rho_1(\boldsymbol{r}, \boldsymbol{r})$ and $n(p)$ is the single-particle momentum distribution. For n=2

$$\rho_2(\boldsymbol{r}_1,\boldsymbol{r}_2,\boldsymbol{r}'_1,\boldsymbol{r}_2)\approx\rho(r_2)\rho_1(\boldsymbol{r}_1,\boldsymbol{r}'_1)\zeta_2(\boldsymbol{r}_1,\boldsymbol{r}'_1;\boldsymbol{r}_2), \tag{9}$$

with the 'off-diagonal' pair-distribution function ζ_2 written as [12]

$$\zeta_2(\boldsymbol{r}_1,\boldsymbol{r}'_1;\boldsymbol{r}_2)\approx\sqrt{g(\boldsymbol{r}_1,\boldsymbol{r}_2)g(\boldsymbol{r}'_1,\boldsymbol{r}_2)} \tag{10}$$

The expression (10) modifies through ζ_2 the Hartree approximation for ρ_2, but neglects the corresponding Fock part which has a longer range.

Effects due to a strong repulsion in V_{NN} are as usual accounted for by a partial summation involving the following off-shell eikonal phase

$$\tilde{\chi}(q,\boldsymbol{r}_1,s)\equiv -i/v_q\Big[\int_0^s ds'V(\boldsymbol{r}-s'\hat{q})-sV(\boldsymbol{r}-s\hat{q})\Big]\rightarrow -i\Big[e^{i\tilde{\chi}(q,\boldsymbol{r}_1,s)}-1\Big] \tag{11}$$

For sufficiently high q, collisions of low multiplicity suffice and in the calculations to be reported, we limited ourselves to the simplest, binary collisions. In a first cumulant representation $\tilde{\Omega}$ in Eq. (7c) reads [11] ($\boldsymbol{r}=\boldsymbol{r}_1-\boldsymbol{r}_2$))

$$\tilde{\Omega}(q,\boldsymbol{r}_1,s)=\int d\boldsymbol{r}\,\rho(\boldsymbol{r}_1-\boldsymbol{r})\zeta_2(\boldsymbol{r},s)\tilde{\Gamma}(q,\boldsymbol{r}_1,s) \tag{12a}$$

$$\tilde{\Gamma}=e^{i(\tilde{\chi}_1+\tilde{\chi}_2)}-1 \tag{12b}$$

The phases $\tilde{\chi}_j$ above correspond to the two terms in (11). $\tilde{\chi}_1$ there is an integral of V over a finite path segment and can be shown to be the off-shell analog of the standard on-shell phase in eikonal theory [17]. The same holds for the corresponding profile $\tilde{\Gamma}_1=e^{i\tilde{\chi}}-1$. For short range interactions it is approximately related to the on-shell analog ($\boldsymbol{r}=\boldsymbol{b},z$)

$$\tilde{\Gamma}_1(\boldsymbol{r},s)\approx\theta(s-z)\theta(z)\Gamma_1(\boldsymbol{b}) \tag{13a}$$

$$\Gamma_1(\boldsymbol{b})\approx\frac{\sigma^{tot}}{2}(1-i\tau)A(b) \tag{13b}$$

Eq. (13b) is a standard parametrization of the profile in terms of σ^{tot}, the total NN cross section, τ, the ratio of real to imaginary part of the elastic NN amplitude and $A(b)$ its range. Although rigorously $\tilde{\chi}_2=-s\frac{\partial}{\partial s}\tilde{\chi}_1$ there appears to be no comparable simple expression for $\tilde{\Gamma}_2=e^{i\tilde{\chi}_2}-1$. We approximate

$$\tilde{\Gamma} \equiv e^{i(\tilde{\chi}_1+\tilde{\chi}_2)} - 1 \approx (1+i\tilde{\chi}_2)s\ e^{i\tilde{\chi}_1} - 1 = \Big(1 - s\frac{\partial}{\partial s}\Big)\tilde{\Gamma}_1, \tag{14}$$

and thus for $\tilde{\Omega}$, Eq. (12),

$$\tilde{\Omega}(q,\boldsymbol{r}_1,s) \approx -\Big\langle \sigma_q^{tot}(1-i\tau_q)/2\Big\rangle \int d^2\boldsymbol{b} A_q(b)$$
$$\Big[\int_0^s dz\rho(\boldsymbol{b}_1-\boldsymbol{b},z_1-z)\zeta_2(b,z,s) - s\rho(\boldsymbol{b}_1-\boldsymbol{b},z_1,s)\zeta_2(b,s,s)\Big] \tag{15}$$

Here and in the following, brackets imply an average over p,n parameters (p,n densities are taken to be the same), thus

$$\Big\langle \sigma^{tot}(1-i\tau)/2\Big\rangle = A^{-1}\Big[Z\sigma_{pp}^{tot}(1-i\tau_{pp})/2 + N\sigma_{pn}^{tot}(1-i\tau_{pn})/2\Big] \tag{16}$$

Eqs. (7c), (8) and (15) provide the elements for a calculation of the structure function $W_{\rm N/A}$ for a nucleus composed of point-nucleons

$$W_{\rm N/A}(q,\nu) = \frac{M}{q}\phi(q,y) \tag{17a}$$
$$\phi(q,y) = \int \frac{d\boldsymbol{p}}{(2\pi)^3} n(|\boldsymbol{p}|) R\Big(q, p_z - y(q,\nu)\Big) \tag{17b}$$
$$R(q,y) = \int \frac{ds}{2\pi} e^{iys} \int d\boldsymbol{r}_1 \rho(\boldsymbol{r}_1) \exp[\tilde{\Omega}(q,\boldsymbol{r}_1,s)] \tag{17c}$$

Eqs. (17) are easily seen to correspond to a local density generalization of the corresponding FSI expression for NM used in [11], but with the parametrization for Γ_2 there replaced by the one implicit in (14). Combination of (1), (2) and (17) produces the total inclusive cross section (ICS) per nucleon

$$\frac{d^2\sigma_{eA}(\epsilon',\theta,Q^2)}{d\Omega d\epsilon'} = \Big(\frac{d\sigma(\epsilon',\theta,Q^2)}{d\Omega}\Big)_{\rm M} \int d\nu' \int \frac{d\boldsymbol{p}}{(2\pi)^3} n(|\boldsymbol{p}|) R\Big(q, p_z - y(q,\nu')\Big)$$
$$\Big\langle W_{2,N}(q,\nu-\nu'+\mathcal{E}_{\boldsymbol{q}}) + 2{\rm tg}^2(\theta/2) W_{1,N}(q,\nu-\nu'+\mathcal{E}_{\boldsymbol{q}})\Big\rangle \tag{18}$$

One notices that the energy loss in the above nucleon structure functions W_N is an integration variable, whereas $\nu = \epsilon - \epsilon'$ in the Mott cross section (Eq. (1)) is fixed. The two therefore do not generally combine into the inclusive cross section for a nucleon. This though is the case for the nucleon-elastic part (i.e. the component of W_N where the nucleon remains

unexcited) and which is our main concern. With barred quantities defined as in (2) one finds (cf. Eqs. (17)

$$\left(\frac{d^2\sigma_{eA}}{d\Omega d\epsilon'}\right)^{N,el} = \left\langle\left(\frac{d^2\bar{\sigma}_{eN}}{d\Omega d\epsilon'}\right)^{N,el}\right\rangle W_{\mathrm{N/A}}[q,y(q,\nu)]$$
$$\left\langle\left(\frac{d^2\bar{\sigma}_{eN}}{d\Omega d\epsilon'}\right)^{N,el}\right\rangle = \left(\frac{d\sigma}{d\Omega}\right)_{\mathrm{M}}\left\langle \bar{W}^{el}_{2,N}(q,\nu) + 2\mathrm{tg}^2(\theta/2)\bar{W}^{el}_{1,N}(q,\nu)\right\rangle \tag{19}$$

In the expression ultimately to be compared with experiment one adds to the elastic part (19) a nucleon inelastic contribution [9,18]

$$\frac{d^2\sigma_{eA}}{d\Omega d\epsilon'} = \left(\frac{d^2\sigma_{eA}}{d\Omega d\epsilon'}\right)^{N,el} + \left(\frac{d^2\sigma_{eA}}{d\Omega d\epsilon'}\right)^{N,inel} \tag{20}$$

As remarked, the above is in essence a NR result with relativistic kinematics. However, in the total FSI phase $\tilde{\Omega}$, Eq. (15), there is no explicit reference to the underlying NR potential model. We then postulate its validity in the relativistic regime.

We first address the N-elastic part (19) in (20) and thus $\phi_A = (q/M)W_{\mathrm{N/A}}$. The input for its calculation is relatively simple:

i) Single-nucleon densities $\rho(r)$, taken to be the same for p, n [19]

ii) Single-nucleon momentum distributions $n(p)$

$$n_1(p) = n_{1,0}\left[e^{-(p/p_1)^2} + \mu e^{-(p/p_2)^2}\right]$$
$$n_2(p) = n_{2,gr}(p) + n_{2,ex}(p) \tag{21}$$

The distribution n_1, with $p_1 = \sqrt{\frac{2}{5}}p_F$; $p_2 = \sqrt{3}p_1$; $\mu = 0.03$; p_F=250 MeV, is one, independent of A [20]. For C and Fe we tested in addition a two-component form n_2, derived from a parallel decomposition of the spectral function [7]. Finally for NM we exploited the result computed in [5].

iii) For the pair-distribution function in the Ansatz (10) for ζ_2 we used $g(r)$ for NM [21]

iv) pp and pn scattering parameters as in Table I of Ref. [11] for $\sigma^{tot}, \tau, A(b)$ in (13).

With quite similar pp and pn scattering parameters and identical single nucleon densities, target specificity of $W_{\mathrm{N/A}}$ is mainly expected from single particle densities and momentum distributions in Eq. (17).

We have computed $\phi(q, y)$ from Eqs. (17) and (15) for C, Al, Fe and Au (He has been disregarded, because of the neglect of core recoil). Figs. 1a,b show $\phi(q, y)$ for Au and NM for some representative values q (in GeV)= 0.50, 2.2, ∞. Reduced responses for other targets practically overlap with $\phi_{\rm Au}$. An insert displays for all targets $\phi_A(q = 2, 2, y)$ the immediate $y \leq 0$ neighbourhood of the QEP.

All reduced responses for relatively low q manifest modest FSI effects as asymmetries around y=0 in the large $|y|$ wings and a small shift in the position of the QEP towards negative y. Those effects vanish rather slowly for increasing q as is typical for, non-confining interactions with strong short-range repulsion [22]. [1]

To the extent that $\phi_A(q, y)$ is close to $\phi_A^{as}(y)$, the target non-specificity of the former is readily traced to the A-independent momentum distribution $n_1(p)$, Eq. (21) in the expression (6) for ϕ_A^{as}. In order to test sensitivity to $n(p)$, we exploit the availability for C and Fe of the two distributions in (21). Fig. 1c shows a $\lesssim$ 10% effect in the QEP and additional differences in the wings.

Finer details in ϕ occur for large negative y, where the response in the binary collision approximation falls below a percent of the peak value at the QEP and occasionally even oscillates around 0. Although $\phi^{exact} \geq 0$, separate components of a response or approximations need not be non-negative. The occasional oscillations in the binary collision approximation for ϕ for large $|y|$, are thus direct proof of the local insufficiency of that approximation. Also without that incontrovertible evidence, small FSI contributions due to binary and multiple

---

[1] Differences between responses for any A and NM are characteristically larger than the same for any two finite nuclei. It reminds one that distributions $n(p)$ for heavy nuclei are not 'close' to the one for NM. We also note that in spite of different statistics and interactions between constituents, and hence entirely different single-constituent momentum distributions, responses of systems, as different as are finite nuclei and liquid He, have remarkably similar shapes. The same has been observed by G. West [23].

collisions are expected to compete for sufficiently large $|y|$.

Next we consider ICS ratios per nucleon under identical kinematic conditions. Using (19) and the near-universality of the reduced responses ϕ_A for nuclei composed of point-nucleons, one has

$$\xi^{th}_{A_1,A_2}(\epsilon,\theta,\nu) \equiv \frac{d^2\sigma_{eA_1}/A_1}{d^2\sigma_{eA_2}/A_2} = \frac{\phi_{A_1}}{\phi_{A_2}} \approx 1, \tag{22}$$

The same ratio can also be extracted from data, and for $A_1, A_2 \geq 12$ one finds confirmed that, within a 10-15 % margin, $\xi^{exp}_{A_1,A_2} \approx 1$. This is a remarkable and vital piece of information because, contrary to the theoretical expression (19), the left-hand side of (22) depends in principle on all kinematic variables ϵ, θ, ν, and on the mass numbers. Disregarding scatter in data where smooth behaviour is expected, systematic deviations occur only for near-elastic, small energy transfer ν regions, or equivalently (for fixed q) regions with large negative y. To those we shall return shortly.

A special case is $A_2 \to \langle N\rangle$. The appropriate ratio (22) then resembles a scaling function and its nucleon-elastic part ($y \lesssim 0$) is from (19) seen to be

$$\bar{\xi}^{n,el}_{A,N} \equiv \frac{d^2\sigma_{eA}/A}{d^2\bar{\sigma}^{N,el}_{e\langle N\rangle}} = \frac{M}{q}\phi_A \tag{23}$$

Figs. 2a,b show for Fe separately, and for C, Al, Fe and Au together the $y<0$ parts of the ratio $\bar{\xi}_{A,N}(q,y)$ extracted from the 4 data sets with ϵ =3.6 GeV. Those are seen to display reasonable quality, universal scaling, i.e. approximate independence on A as well as on q. Fig. 2c displays $\bar{\xi}$ for NM; its relevance will be discussed below. For NM, as well as for real targets, the quality of scaling in y (5) appears to be appreciably better than in a scaling variable, appropriate to the PWIA [2,25]. [1]

The close agreement between experimental and computed ICS ratios does not imply the same for the cross sections themselves. In the study of the latter one is nevertheless guided

[1]Another special case is $\xi_{A,D}$, Eq. (22), as function of Q^2 and the Bjorken variable $x = Q^2/2M\nu$ for $x \gtrsim 1$ ($y \lesssim 0$) between the QEP and the elastic threshold. Particular emphasis has been placed on the range $1.9 \gtrsim x \gtrsim 1.4$, where $\xi_{A,D}$ reaches a plateau value 5-6, far in excess of $\xi_{A_1,A_2} \approx 1$

by the result (22), which strongly limits the information present in the complete body of data.

Fig. 3a thus presents data for Al, Au, $\epsilon = 3.6$ GeV, $\theta = 25°$. Drawn and dashed curves are predictions for Al and Au respectively. Fig. 3b gives the ICS per nucleon for Fe, $\epsilon = 3.6$ GeV, $\theta = 16°$. The solid and dashed curves there are results, using the two distributions in (21). One notes discrepancies in the region of small ν which, for approximately fixed q, corresponds to the large negative y wing of $W_{\rm N/A}$ (cf. Figs. 1). That region has been shown to be sensitive to details in $n(p)$ and to higher order FSI. The former is apparent in Fig. 1a and it is interesting that for the kinematic conditions for Fe relevant to Fig. 3b, the data fall in between the two predictions.

Fig. 3c gives another set of Fe data for $\epsilon = 3.6$ GeV, $\theta = 25°$. Along our predictions (drawn and dashed curves as in Fig. 3b) we inserted the DWIA prediction of Sick et al [8]: For small ν those overestimate the data by an order of magnitude, in contradistinction to our slight overestimate. The authors above report colour transparency, suppressing purely hadronic FSI (hatched area there).

Finally we show in Fig. 3d for ϵ=3.6 GeV, $\theta = 30°$ extrapolated pseudo-data as well as predictions for symmetric NM and observe good agreement down to the smallest measured ν. In view of the above one is tempted to link this with the single-nucleon momentum distribution which has been accurately calculated for NM [5,28]. Here too we show the DWIA result [9] and the claimed colour transparency reduction.

---

for *any* two targets with $A_1, A_2 \geq 4$. First, on purely kinematic grounds $\xi_{A,D}$ grows towards the D elastic limit x=2. Far more important is the off-the-mean spatial extension of D. Indeed the height of the plateau of $\xi_{A,D}$ simply reflects the dissimilarity for D and A of the density ρ and ρ_2 in (19): it contains no other information. Similar, though less outspoken deviations of ICS ratios, occur for $\xi_{A,{\rm He}}$ referring to the uncharacteristically compact ^{4}He: ratios are ≈ 1.5 for medium x, approaching $\approx$2 for $x \to 2$ [3].

The generally satisfactory agreement between data and our predictions is as good as may be expected for any calculation of hadron observables with natural imperfections in the underlying theory as well as in the quality of input.

We have already mentioned the PWIA as the conventional starting point for the treatment of inclusive scattering and one is drawn to a comparison. There appear to be clear advantages in the approach starting from the asymptotic limit. From a technical point of view, the input is far simpler, as is for instance manifest in the required momentum distribution as opposed to the two-variable spectral functions. Of greater importance are essential differences:

1) Our treatment is free of off-shell problems inherent to perturbative PWIA.

2) Starting from the DWIA [8,9] no simple argument explains the observed approximate universality of the data.

3) The relative contribution of FSI to the total ICS is appreciably larger for the PWIA than for the asymptotic limit as starting point (cf. Fig. 3 in [9]). This is also reflected in the quality of scaling. In using a relativistic West scaling variable y, one apparently includes part of the FSI beyond the PWIA approximation (see [30] for a recent example in the relativistic domain).

In the end predictions for the low-ν region based on hadron dynamics appear to differ considerably. The overestimate of the retained hadronic DWIA is reported to be off-set by colour transparency [9] (see below).

We summarize our study of inclusive scattering of electrons from nuclei in the few-GeV region, where the basic total nuclear structure function has been represented as a folding of structure functions W_N of a nucleon at rest, and $W_{\rm N/A}$ for a nucleus composed of point-particles.

We focussed on the nucleon-elastic region of W_N, for which the eA inclusive cross section factors in the elastic eN cross section and the response $W_{\rm N/A}(q,y)$ for a nucleus composed of point-nucleons. The reduced response $\phi_A(q,y)=(q/M)W_{\rm N/A}(q,\nu)$ appears to be a nearly universal function, independent of A and of the momentum transfers q, leaving only a

modest role for FSI over and above the asymptotic limit. An immediate consequence is the approximate target independence of inclusive cross sections per nucleon, which is also borne out by experiment. A second consequence is the allocation of the strong variation in the eA cross section to the same in eN. The Ansatz (2) provides a simple explanation for the observed regularities. Calculations produce throughout satisfactory agreement with the ICS data.

Regarding details we checked the influence of different single-nucleon momentum distributions and found relatively large effects for low ν ICS. We also emphasized the good agreement obtained for nuclear matter ICS down to the small-ν region and mentioned the possible relation with a computed momentum distribution, available for that substance.

A second agent which in principle contributes to ICS for low-ν are FSI due to multiple collisions between the knocked-on and core nucleons. Those we emphasize, are part of the description using Glauber theory and a reliable calculation is definitely required. Rather than questioning the validity of Glauber theory for low-ν ICS [8], we blame discrepancies there to imperfections in the application of a theory, formulated in terms of hadronic degrees of freedom. In particular we do not find evidence for colour transparency effects [8,9], nor are such effects expected for the relatively low Q^2 involved.

The authors thank S.A. Gurvitz for a critical reading of the ms.

REFERENCES

[1] D.B. Day *et al*, Phys. Rev. Lett. **43** 1143 (1979).

[2] D.B. Day *et al*, Phys. Rev. Lett. **59** (1987) 427.

[3] D.B. Day *et al*, Phys. Rev. C**48**, (1993) 1849.

[4] D.B. Day *et al*, Phys. Rev. Lett. C**40**, 1011 (1989).

[5] e.g. O.Benhar, A. Fabrocini and S. Fantoni, Nucl. Phys. A**505** (1989) 367.

[6] C. Ciofi degli Atti, E. Pace amd G. Salmè, Phys. Rev. C**43** (1991) 1155.

[7] C. Ciofi degli Atti, D.B. Day and S. Liuti, Phys. Rev. C**46** (1994) 1045.

[8] I. Sick, S. Fantoni, A. Fabrocini and O. Benhar, Phys. Lett B**323** (1994) 267; Nucl. Phys. A**579**, (1994) 493.

[9] O. Benhar, A. Fabricioni, S. Fantoni, G.A. Miller, V.R. Pandharipande and I. Sick, Phys. Rev. C**44** (1991) 2328.

[10] C. Ciofi degli Atti and S. Simula, Phys. Lett. B**325** (1994) 276.

[11] A.S. Rinat and M.F. Taragin, Nucl. Phys. A **571** (1994) 733.

[12] H.A. Gersch, L.J. Rodriguez and Phil N. Smith, Phys. Rev. A**5**, (1973) 1547; H.A. Gersch and L.J. Rodriguez, Phys. Rev. A**8** (1973), 905.

[13] e.g. R.J. Jaffe, Nucl. Phys. A**478** ((1988) 3c; P.J. Mulders, A.W. Schreiber and H. Meyer, Nucl. Phys. A**549** (1992) 498.

[14] S.A. Gurvitz and A.S. Rinat, TR-PR-93-77/ WIS-93/97/Oct-PH; Progress in Nuclear and Particle Physics, Vol. 34 (1995), to be published.

[15] S.A. Gurvitz, Phys. Rev. C**42** (1990) 2653.

[16] J. Negele and D. Vautherin, Phys. Rev. C**5**, (1972) 1472; *ibid* Phys. Rev. C**11**, (1974)

1031.

[17] e.g. A.S. Rinat and M.D. Taragin, Phys.Lett. B**267** (1991) 447.

[18] A. Bodek and J.L. Ritchie, Phys. Rev. D**23** (1981 1070.

[19] H. de Vries, W.D. de Jager and C.de Vries, Nucl. Data Tables **36**, (1987) 495.

[20] A. Kohama, K. Yazaki and R. Seki, Nucl. Phys. A**536** (1992) 716; *ibid* A**551** (1993) 687.

[21] R. Wirenga, private communication.

[22] S.A. Gurvitz and A.S. Rinat, Phys. Rev. C**47** (1993) 2901.

[23] G. West, private communication.

[24] S. Rock et al, Phys. Rev. Lett. **49** (1982) 1139; R.G. Arnold et al *ibid* **61** (1988) 806.

[25] e.g. C. Ciofi degli Atti, E.Pace and G. Salme, Phys. Rev. C**43** (1991) 1155.

[26] S. Liuti, Phys. Rev. C**47** (1993) 1854.

[27] O. Benhar, A. Fabricioni, S. Fantoni and I. Sick. Phys. Lett. B**343** (1995) 47.

[28] B.E. Vonderfecht, W.H.D. Dickhoff, A. Polls and A. Ramon, Nucl. Phys. A **555** (1993) 1.

[29] L.L. Frankfurt, M.I. Strikman, D.B. Day and M. Sargsyan, Phys. Rev. C**48** (1993) 2451.

[30] S.A. Gurvitz, preprint WIS-95/6-Febr-PH.

Figure captions

Fig. 1a. The reduced structure function $\phi_A(q,y) = (q/M)W_{\rm N/A}(q,\nu)$, Eq. (17), for Au. The drawn, dashed and dotted curves correspond to, q(GeV)=0.5, 2.2, ∞. The insert gives the small $y \le 0$ parts of $\phi_A(2.2,y)$ for a number of targets.

Fig. 1b. Same as Fig. 1a for nuclear matter (NM).

Fig. 1c. Same as Fig. 1a for Fe, using the momentum distributions n_1 (drawn line) and

n_2 (dashed line) in (22).

Fig. 2a. The cross section ratio $\bar{\xi}_{A,N}$, Eq. (22), as function of y for Fe, ϵ=3.6 GeV and 4 scattering angles, showing empirical y-scaling.

Fig. 2b. Same as Fig. 2a for all targets, displaying approximate universal scaling.

Fig. 2c. Same as Fig. 2a for symmetric NM.

Fig. 3a. ICS, Eq. (20), for Al (squares), Au (crosses), ϵ=3.6 GeV, $\theta = 25°$. Drawn and dashed curves correspond to Al and Au.

Fig. 3b. Same as Fig. 3a for Fe, $\theta = 16°$. Drawn and dashed lines are predictions for the two momentum distributions n_1, resp. n_2 in (22).

Fig. 3c. Same as Fig. 3b for $\theta = 25°$. The hatched area gives the reported reduction of the dot-dashed DWIA results due to colour transparency [8].

Fig. 3d. Same as Fig. 3c for NM for $\epsilon = 3.6$ GeV, $\theta = 30°$ [9].

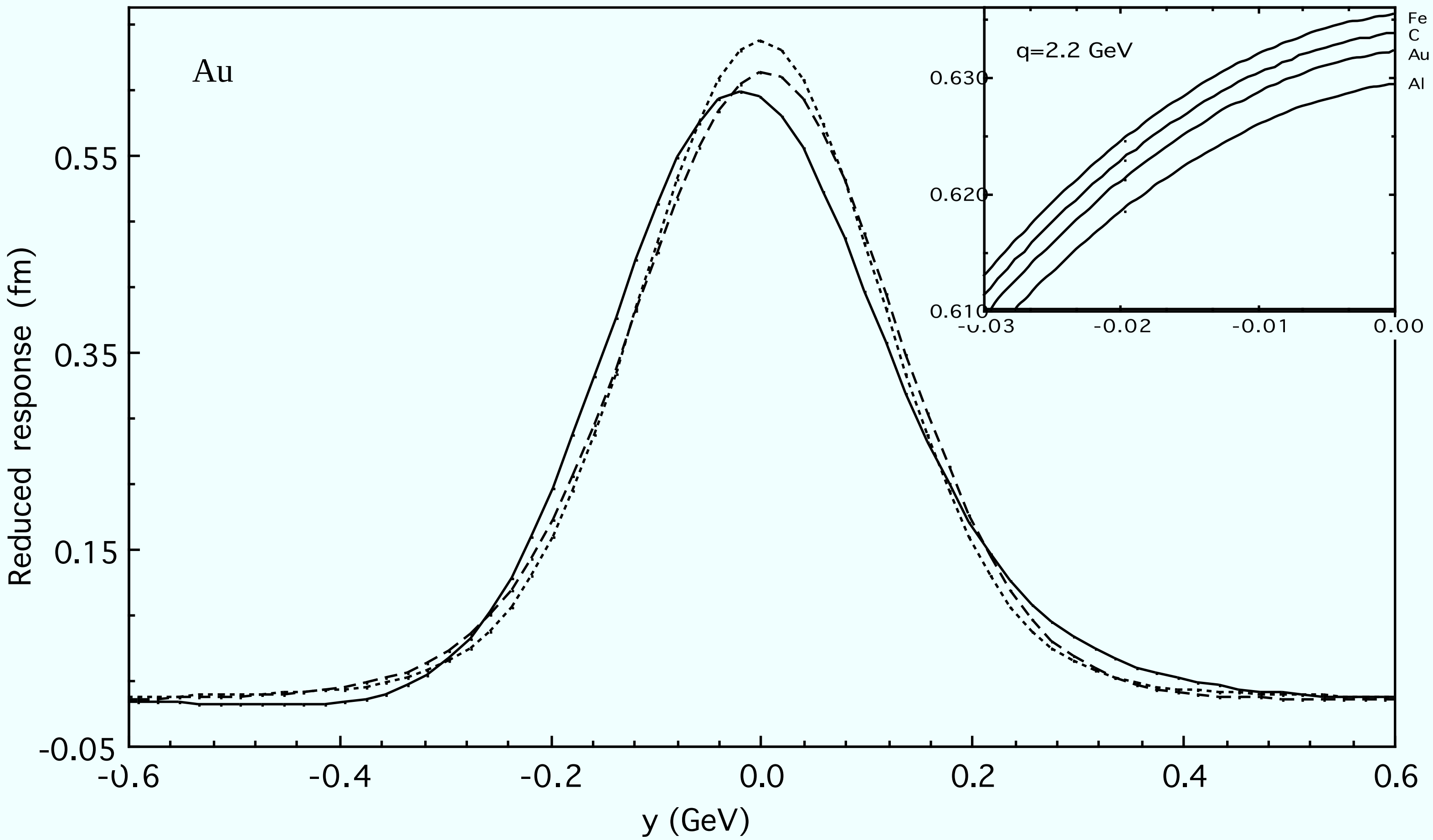

Au
Reduced response (fm)
y (GeV)
-0.05
0.15
0.35
0.55
-0.6
-0.4
-0.2
0.0
0.2
0.4
0.6
q=2.2 GeV
0.610
0.620
0.630
-0.03
-0.02
-0.01
0.00
Fe
C
Au
Al

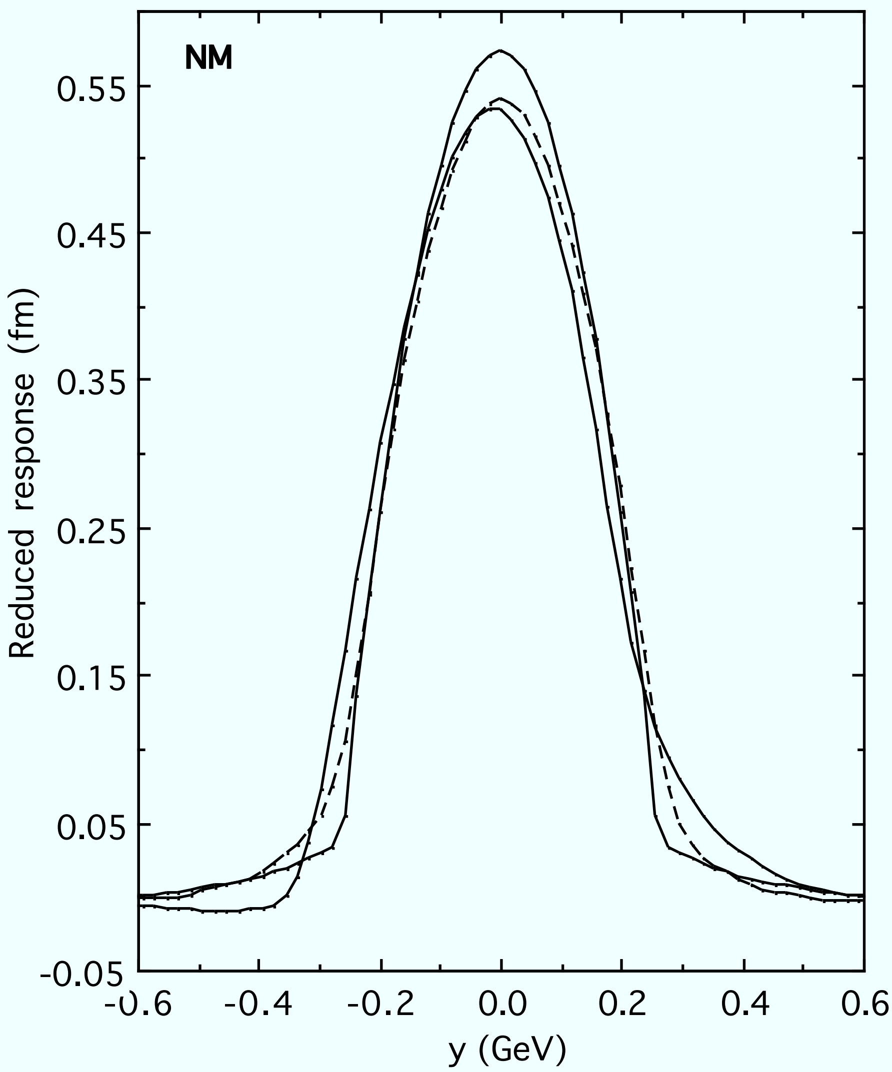

NM
Reduced response (fm)
0.55
0.45
0.35
0.25
0.15
0.05
-0.05
-0.6
-0.4
-0.2
0.0
0.2
0.4
0.6
y (GeV)

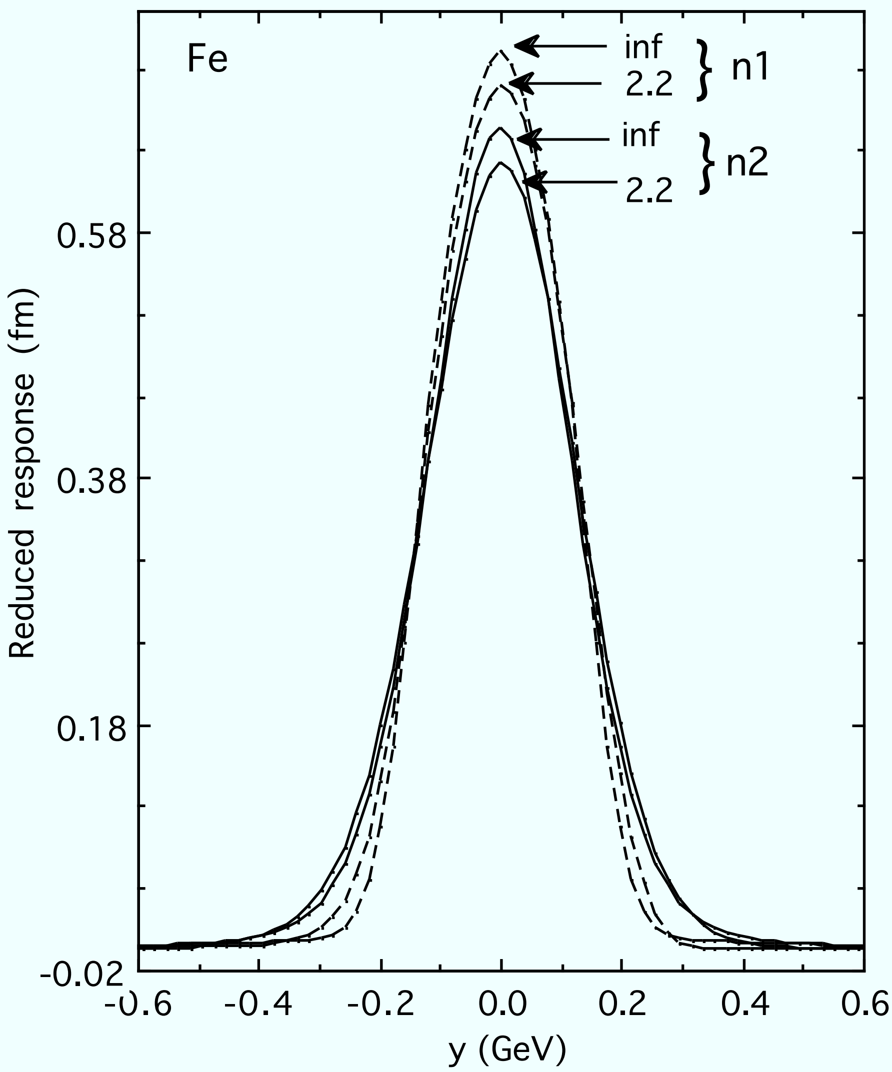

Fe
inf
2.2
n1
inf
2.2
n2
0.58
0.38
0.18
-0.02
Reduced response (fm)
-0.6
-0.4
-0.2
0.0
0.2
0.4
0.6
y (GeV)

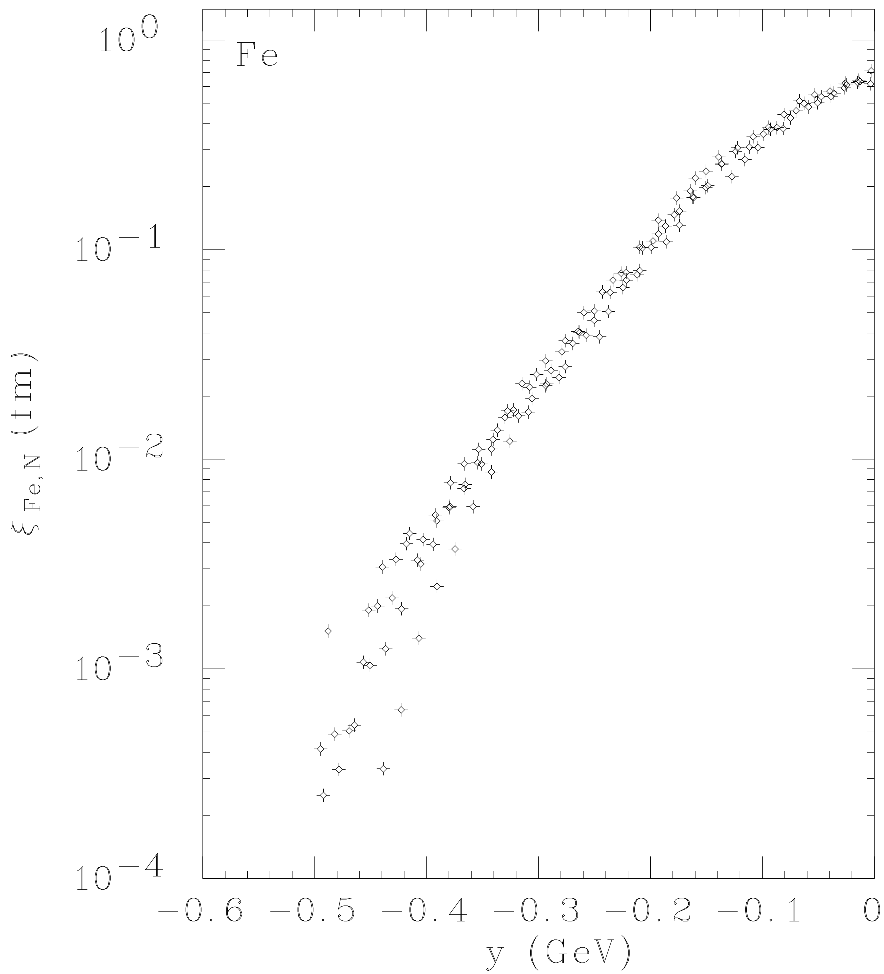

Fe
10^{0}
10^{-1}
10^{-2}
10^{-3}
10^{-4}
$\xi_{Fe,N}$ (fm)
−0.6 −0.5 −0.4 −0.3 −0.2 −0.1 0
y (GeV)

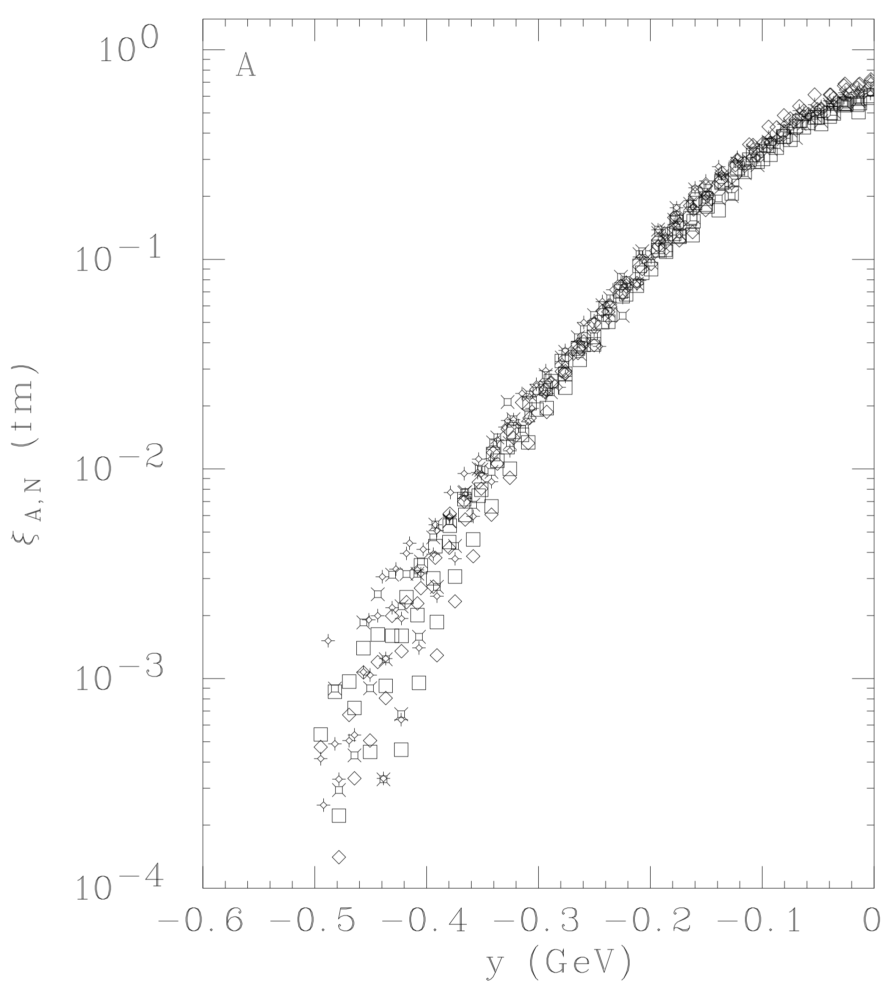
A
$\xi_{A,N}$ (fm)
10^0
10^{-1}
10^{-2}
10^{-3}
10^{-4}
−0.6 −0.5 −0.4 −0.3 −0.2 −0.1 0
y (GeV)

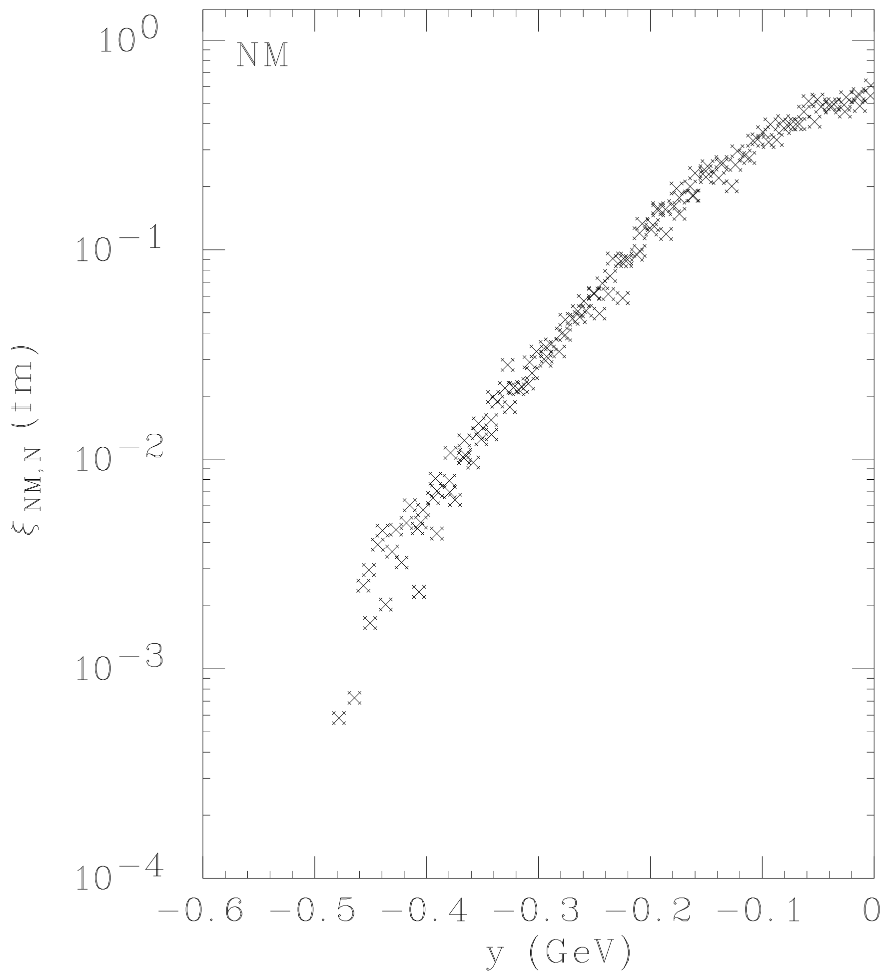

NM
$\xi_{NM,N}$ (fm)
10^{0}
10^{-1}
10^{-2}
10^{-3}
10^{-4}
−0.6 −0.5 −0.4 −0.3 −0.2 −0.1 0
y (GeV)

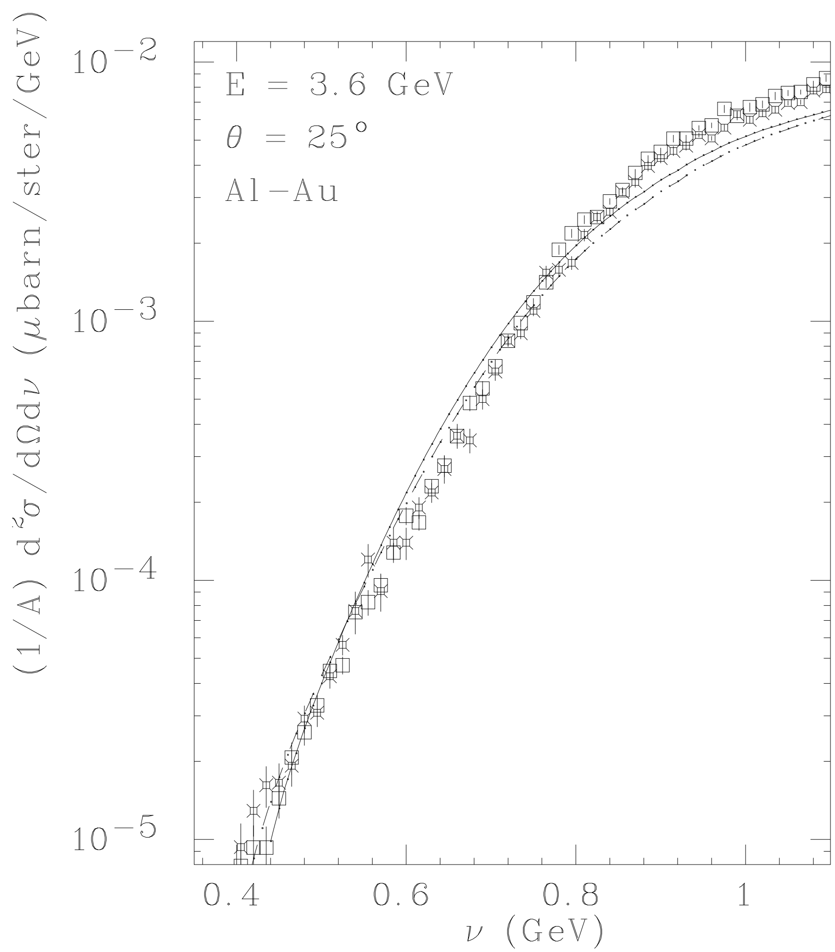

E = 3.6 GeV
θ = 25°
Al−Au
10−2
10−3
10−4
10−5
(1/A) d²σ/dΩdν (μbarn/ster/GeV)
0.4
0.6
0.8
1
ν (GeV)

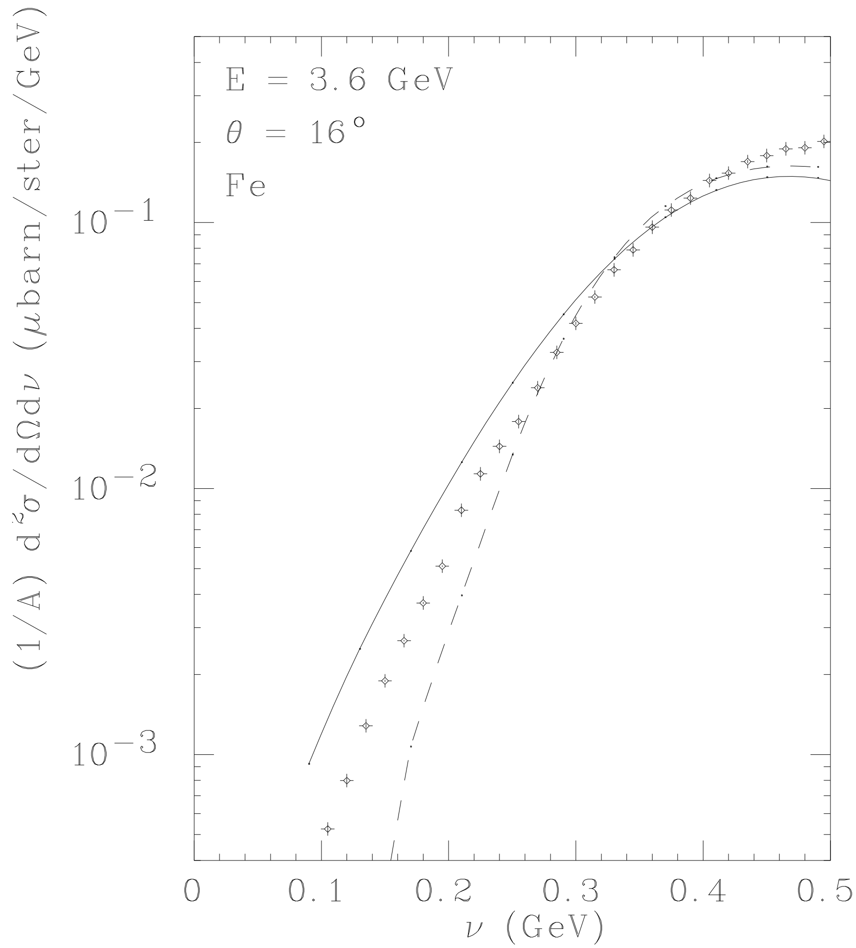
E = 3.6 GeV
θ = 16°
Fe
(1/A) d²σ/dΩdν (μbarn/ster/GeV)
10⁻¹
10⁻²
10⁻³
0
0.1
0.2
0.3
0.4
0.5
ν (GeV)

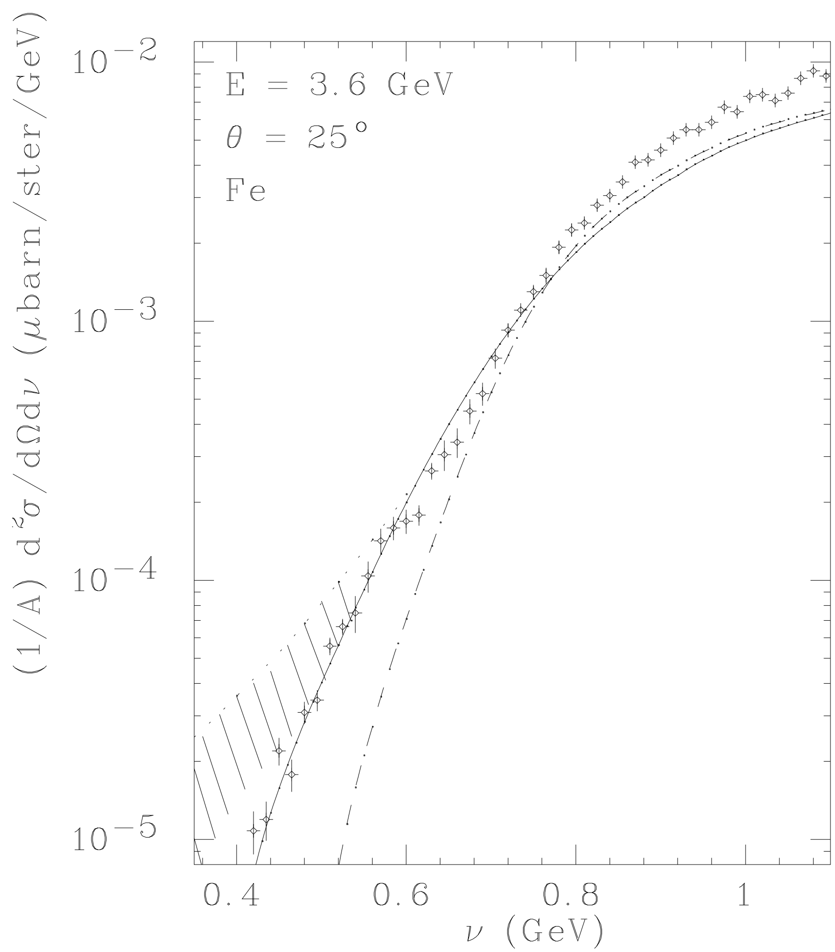
E = 3.6 GeV
θ = 25°
Fe
(1/A) $d^2\sigma/d\Omega d\nu$ (μbarn/ster/GeV)
10^{-2}
10^{-3}
10^{-4}
10^{-5}
0.4
0.6
0.8
1
ν (GeV)

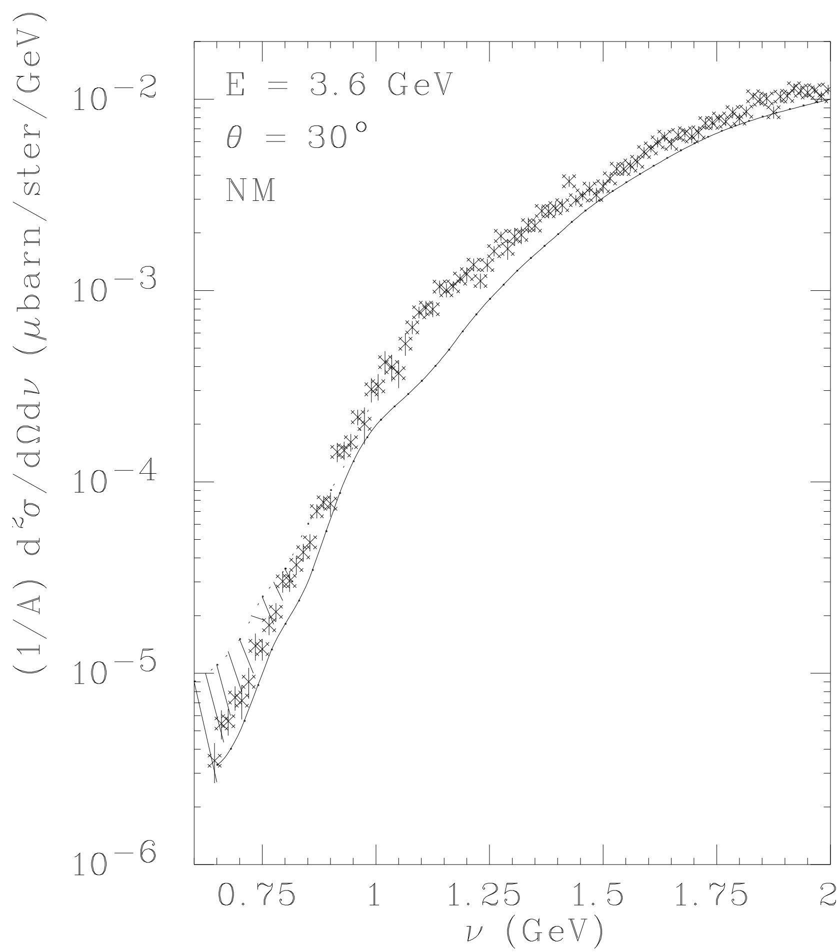

E = 3.6 GeV
θ = 30°
NM
(1/A) d²σ/dΩdν (μbarn/ster/GeV)
10−2
10−3
10−4
10−5
10−6
0.75
1
1.25
1.5
1.75
2
ν (GeV)